

S.M. KOSTRITSKII¹✉
P. BOURSON²
M. AILLERIE²
M.D. FONTANA²
D. KIP³

Quantitative evaluation of the electro-optic effect and second-order optical nonlinearity of lithium tantalate crystals of different compositions using Raman and infrared spectroscopy

¹ MPTE Dept., Moscow Institute of Electronic Technology, Moscow, 124498, Zelenograd, Russia
² Lab. Matériaux Optiques, Photonique et Systèmes, UMR CNRS 7132, University of Metz and Supelec, 2 rue E. Belin, 57070 Metz, France
³ Clausthal University of Technology, Institute of Physics and Physical Technologies, Leibnizstr. 4, 38678 Clausthal-Zellerfeld, Germany

Received: 25 July 2005 / Revised version: 20 September 2005
© Springer-Verlag 2005

ABSTRACT Nominally pure lithium tantalate (LiTaO_3) crystals with different chemical compositions were characterized by Raman scattering, infrared reflection, and infrared absorption spectroscopy. In these crystals specific phonon bands are correlated to electro-optic and nonlinear optical properties. The electro-optic and nonlinear optical coefficients were determined and the data are compared with literature values obtained by direct measurements. Our measurements are in good accordance with the literature data, which opens up a new possibility for fast and easy estimation of electro-optic and nonlinear optical performance of newly developed LiTaO_3 -based materials modified by stoichiometry.

PACS 42.70.Mp; 78.20.Jq; 78.30.-j

1 Introduction

Lithium tantalate (LiTaO_3) is an attractive material for nonlinear and integrated optics. Its large electro-optic and nonlinear coefficients are comparable to those of lithium niobate (LiNbO_3) and its high threshold for photorefractive damage is known to be more than an order of magnitude larger than that of LiNbO_3 for visible light [1]. Guided-wave devices implemented in this material have exhibited a much higher power handling capability [2–4] than those in LiNbO_3 , making them ideal for a variety of high-throughput applications. LiTaO_3 crystals, however, can be grown in a comparably wide composition range [5, 6], where Li deficits up to about 4% with respect to the stoichiometric composition are possible. As most of the physical properties should depend on composition when regarding the general analogy [7–9] with LiNbO_3 , it is necessary to check the Li content by appropriate (preferably nondestructive) methods. Therefore, a full characterization of the electro-optic, nonlinear-optic and related properties of LiTaO_3 over the entire composition range is necessary.

It has been found [10, 11] that for many materials, including LiTaO_3 and LiNbO_3 , ionic and electronic contributions

to the electro-optic and nonlinear-optical coefficients may be determined from Raman and infrared (IR) reflection spectroscopy data with an accuracy comparable to that of standard direct measurements. The optical and electrical requirements on a material for quantitative Raman and IR reflection spectroscopy data acquisition are often much less stringent, thus this method was established [11] to be an attractive alternative to direct measurement of such coefficients. In particular for new materials, where available samples are often unsatisfactory in size or quality for any but the crudest direct measurements. Additionally, these spectroscopic methods are less time consuming than the straightforward ones. Advantageously, the process of data acquisition with Raman and IR reflection spectroscopy is more tolerant to possible imperfections in the material under test, which typically manifest themselves as optical and electrical inhomogeneities [12].

The high efficiency of this method in the case of bulk materials has been also demonstrated for the characterization of waveguiding layers and recently applied in the case of (annealed) proton-exchanged (PE/APE) LiNbO_3 waveguides [13]. Raman and IR reflection measurements can provide direct information on phonon spectra related to structure and chemical bonds of a given crystal [14–16]. Such information may be useful for a correct identification of both chemical composition and microscopic mechanisms responsible for many physical properties.

In the present study, we have examined Raman and IR reflection spectra for LiTaO_3 crystals with different chemical compositions. The obtained results demonstrate substantial changes of electro-optical and nonlinear-optical properties, crystal disorder, spontaneous polarization, and birefringence with the variation of the chemical composition of nominally pure (undoped) LiTaO_3 crystals.

2 Experimental: Samples and characterization methods

In our study we used the following crystals: (1) pieces of Z- and X-cut wafers (0.5 and 1 mm thick) of nominally pure quasi-congruent LiTaO_3 (47.88 ± 0.04 mol % Li_2O) supplied by Deltronic Crystal Industries [17], (2) bulk samples with a typical size of $(2 \times 3 \times 1)$ mm³ with a composition of 47.2 mol % Li_2O , which is below the congruent composition, i.e. so-called under-congruent crystals, (3) X-

✉ Fax: +7-095-5369934, E-mail: skostritskii@optolink.ru

cut plates ($(0.5 \times 5 \times 4) \text{ mm}^3$) of nominally pure congruently melting crystals grown by the crystal growth team of Osnabrück University [17] from a melt with composition of $48.50 \pm 0.04 \text{ mol \% Li}_2\text{O}$, (4) Z- and X-cut plates of nearly stoichiometric ($49.97 \text{ mol \% Li}_2\text{O}$) LiTaO_3 single crystals fabricated by the vapor transport equilibration (VTE) technique [18, 19] from congruent samples with dimension of $4 \times 5 \times 0.5$ and $0.5 \times 5 \times 4 \text{ mm}^3$, and (5) X-cut plates of under-congruent crystals grown from a melt with $48.15 \text{ mol \% Li}_2\text{O}$ in specific experimental conditions. The surfaces of all samples studied were optical-grade polished and all surfaces were perpendicular to the corresponding crystallographic axes. It should be noted, that we have taken into account the findings reported in [6], where the congruent composition of LiTaO_3 was determined to be less than or equal to $47.7 \text{ mol \% Li}_2\text{O}$. It has been shown, that with the Czochralski growth process applied under specific conditions, a melt composition of $48.39 \text{ mol \% Li}_2\text{O}$ yielded grown crystals of a uniform solid composition of $47.85 \text{ mol \% Li}_2\text{O}$, which is called by us the quasi-congruent composition. This incongruent crystallization of compositionally uniform LiTaO_3 is due to Li rejection from the growth interface exactly balancing Li losses from the melt surface [6]. At the same time, values ranging from 48.3 to $48.5 \text{ mol \% Li}_2\text{O}$, i.e. around the specific melt composition, were reported by many researchers [5, 7–9, 18–20] as the true congruent solid composition. Thus, an evident contradiction takes place for definition: what is the true solid congruent composition for LiTaO_3 single crystals?

A Labram Jobin-Ivon spectrometer was used for micro-Raman and confocal luminescence experiments. Radiation of a He-Ne laser (632.8 nm) is focused by microscopic objectives (magnifications $\times 20$, $\times 50$, and $\times 100$) on the crystal surface. A back-scattering scheme is used to detect the Raman signal through a confocal hole, allowing extraction of light scattered from an extremely small region (diameter is $1.6 \mu\text{m}$ and depth is $4 \mu\text{m}$ when using the microscopic objective $\times 100$) of the crystal. Thus, we are able to detect Raman or luminescence signals from a very small focal area, where extremely high intensities are available even at small input powers.

To measure the IR reflection and IR absorption spectra, we use two spectrophotometers “Bruker IFS 113” and “Specord M80” with standard attachments. All spectra discussed in this paper will be described by notations of the following example [16], e.g., $Z(XY)\bar{Z}$, where the directions inside the parentheses signify the polarizations of the incident and scattered beams, respectively. The letter preceding and following the parenthesis indicates the respective directions of the incident and scattered beams, and \bar{Z} means an opposite direction to the Z direction, as we used the back scattering geometry.

3 Evaluation of crystal compositions of the samples studied

It was already mentioned that there is a contradiction between definitions of the true congruent composition of LiTaO_3 crystals in the literature [5–9, 18, 19] and vendors’ specifications [17, 20, 21]. As a consequence, the data on composition of all nonstoichiometric crystals are rather relative, because different composition calibrations have been

applied by the suppliers of the crystals used in our study. Therefore, to have the possibility of using previous data on various crystal properties as a reference, we first discuss the exact composition of each studied crystal.

In LiTaO_3 , the linewidth of some Raman bands (e.g., $E(\text{TO})$ phonon mode at 142 cm^{-1} , $E(\text{TO})$ phonon mode at 592 cm^{-1} and $A_1(\text{TO})$ phonon modes at 201 and 600 cm^{-1}) can be correlated to the composition (i.e. to $[\text{Li}_2\text{O}]$, or to the composition parameter $x_c = \{[\text{Li}_2\text{O}]/([\text{Li}_2\text{O}] + [\text{Ta}_2\text{O}_5])\} \times 100\%$) of LiTaO_3 crystals [14]. Additional information about disorder arising in the ferroelectrics chains Ta–O can be obtained from weak and broadened features [11–14], in the spectral range between 550 – 900 cm^{-1} , see Figs. 1 and 2.

We have investigated in detail the Raman scattering spectra of all nominally pure single domain LiTaO_3 crystals with different compositions, i.e. with 5 values of x_c ranging from 47.2 (under-congruent crystals) to $\cong 50 \text{ mol \%}$ (nearly stoichiometric crystals). The x_c values were estimated by precision measurements of the linewidth γ of a phonon band in the Raman spectra of our single crystals in Fig. 1, using data about

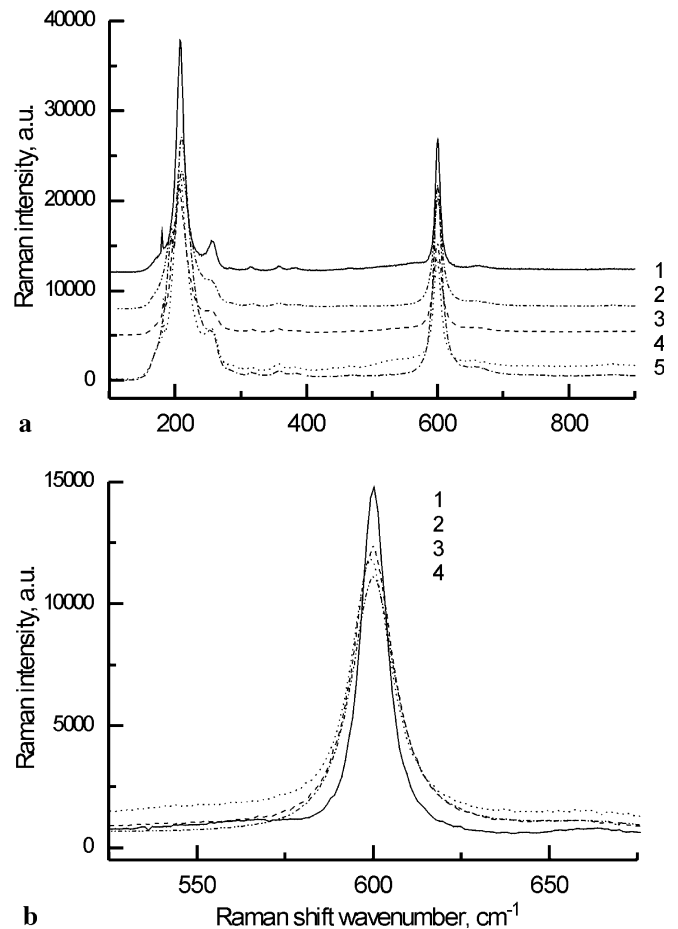


FIGURE 1 (a) Raman spectra measured in scattering geometry $X(ZZ)\bar{X}$ for different LiTaO_3 for (1) nearly stoichiometric SLT, (2) under-congruent UC2, (3) congruent CLT, (4) under-congruent UC1, and (5) quasi-congruent QC crystals. The spectra 1–3 are shifted in the vertical direction for convenience of view; (b) fragment of the Raman spectra of different LiTaO_3 crystals: (1) nearly stoichiometric SLT, (2) congruent CLT, (3) under-congruent UC1, and (4) quasi-congruent QC crystals. Number sequence is given in order of peak intensity reduction at 600 cm^{-1}

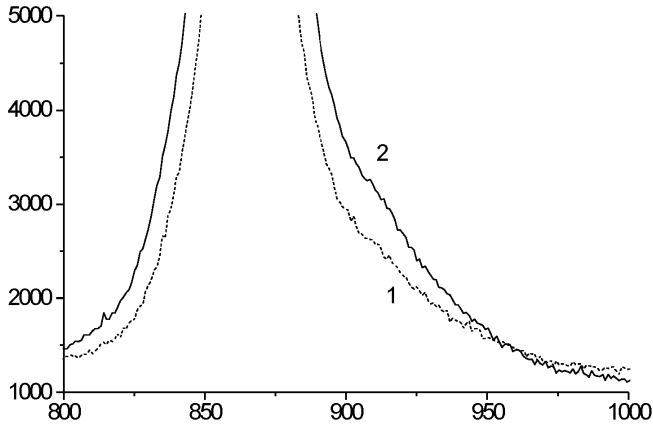


FIGURE 2 Fragment of the Raman spectra measured in scattering geometry $Z(YY)\bar{Z}$ for the congruent CLT (1) and under-congruent UC1 (2) crystals. Note, that the extra band at 907 cm^{-1} (high-wavenumber shoulder of the main band of $A_1(\text{LO})$ phonon at 864 cm^{-1}) is not observed in the spectra of the nearly stoichiometric crystal SLT

the dependence of γ on x_c [14], and the analogy with the general law established for a composition dependence of Raman linewidths in LiNbO₃ crystals [22].

From this data on line shape, using a best-fit procedure with Lorentzian curves to interpolate the data, we find experimental parameters for the modes E and A_1 , and by extracting the width of the apparatus function from these values we have obtained the true linewidth parameters reported in Table 1. The changes in the Raman spectra are caused by an increase of intrinsic defect concentrations, such as $[\text{Ta}_{\text{Li}}]$ and $[\text{V}_{\text{Li}}]$ with $[\text{Li}_2\text{O}]$ reduction. Ta_{Li} is the most important intrinsic defect of LiTaO₃, as Ta_{Li} affects different properties of LiTaO₃ crystals. The substitution of Li by Ta reduces the translational symmetry of the lattice, and changes ionic masses and force constants. Each of these effects contributes to the linewidths of the lattice modes. As the compensation by Ta ions is proportional to the amount of missing Li ions, the Li deficit should show up linearly in the variation of the mode linewidths, similar to LiNbO₃ crystals [22]. Therefore, Raman scattering spectroscopy may be used for an accurate quantitative determination of the chemical composition of LiTaO₃. However, the absolute accuracy of this method depends on the exactness of the concentration data C_{Li} (i.e. $[\text{Li}_2\text{O}]$) for the crystals used as calibration standards. To plot a calibration dependence $C_{\text{Li}}(\gamma)$ at least two fixed points with significantly different C_{Li} are needed. One of the standard crystals (SLT) had been brought to the near stoichiometric composition by vapor transport equilibration (VTE) treatment. The accuracy of the composition is assumed to be

about 0.01% [18, 19], so we take this crystal as the first reference. We used the two crystals referred as QC and CLT, which have different compositions, as second points for the calibration. Consequently, we have obtained two different calibration curves, giving the results as indicated in Table 1. When comparing the obtained compositions with published data on basic crystal properties, the results obtained with the calibration #1 are better correlated with this previous data, so this one is chosen for the further discussion of crystal properties here. However, the results obtained with calibration #2 (that is based on a so-called congruent crystal) may be useful for understanding the differences between the two main approaches used for the definition of a true congruent composition. Thus, the results obtained here for two calibrations may be used to establish useful interrelations between some contradictory data on compositions of the crystals grown with different techniques.

It is important to note, that in nonstoichiometric LiNbO₃, the relaxation around Nb_{Li} antisite defects and Li cation vacancies leads to the formation of small regions with ilmenite-like structure [25, 26]. The structures of ilmenite and LiNbO₃ are very similar and differ only by their cation staking sequence with the regular structure. Computer simulations have shown that the two LiNbO₃ structures have similar stability [26] and, thus, an intermixing of both seems to be possible. This effect, leading to qualitative changes in the phonon spectrum of LiNbO₃, is even more convincing than a simple variation of the linewidths [27]. The basic similarity between structures [7] and phonon spectra [10, 11] of LiNbO₃ and LiTaO₃ crystals allows expectation of the same intermixing in nonstoichiometric LiTaO₃.

Our Raman studies of LiTaO₃ crystals with under-congruent and quasi-congruent compositions have confirmed the presence of the structures intermixing. In the obtained spectra numerous weak lines have been detected in addition to the known phonon spectrum of LiTaO₃. Some of these lines ($186, 401, 458, 661, 751\text{ cm}^{-1}$) were observed earlier in congruent LiTaO₃ crystals and have been assigned to A_2 symmetry phonons, which are forbidden by selection rules for crystals with C_{3v} symmetry [27]. The experimental measurement indicates, that the intensities of these lines are proportional to the Li_2O deficit. A similar dependence on x_c is observed for other lines at $569, 826, 844,$ and 907 cm^{-1} , see Fig. 1. This allows attribution of these lines to regions with ilmenite-like structure. Thus, the entire Raman spectrum of any nonstoichiometric LiTaO₃ crystals can be understood as overlapping spectra of main and ilmenite-like structures.

One of the under-congruent crystals (UC2) shows anomalous features in the Raman spectra. Here numerous weak extra

Crystal	γ_1	γ_2	vendors' $[\text{Li}_2\text{O}]$	$[\text{Li}_2\text{O}]$ our data calibration 1	$[\text{Li}_2\text{O}]$ our data calibration 2
under-congruent 1 (UC 1)	14.2	22.8	47.20 ± 0.06	47.23 ± 0.07	47.66 ± 0.07
under-congruent 2 (UC 2)	12.9	20.9	48.12 ± 0.05	47.75 ± 0.07	48.10 ± 0.07
quasi-congruent (QC)	12.6	20.5	47.88 ± 0.04	47.88*	48.21 ± 0.07
congruent (CLT)	11.8	18.6	48.50 ± 0.04	48.22 ± 0.05	48.50*
stoichiometric (SLT)	7.6	11.9	49.97 ± 0.01	49.97*	49.97*

* these values are used as fix points for the calibration lines

TABLE 1 Raman linewidths γ_1 and γ_2 (given in cm^{-1}) for lines at 600 and 201 cm^{-1} , respectively, for different crystals. The values of the chemical composition $[\text{Li}_2\text{O}]$ (in mol%) were evaluated by using two different calibrations from these Raman data and are compared with literature data published by vendors

specific lines appear connected with sharp changes of intensities and linewidths when compared to the common phonon spectrum of LiTaO_3 . Note, that similar anomalous changes in the Raman spectra were observed in congruent LiNbO_3 crystals after their thermally-induced decomposition, when small micrograins of LiNb_3O_8 appear [29]. Thus, we may reasonably assume, that there are micrograins of LiTa_3O_8 in the crystal UC2 due to an instability of the under-congruent solid composition during the post-growth cooling down process.

The conclusions obtained by analysis of Raman spectra concerning the intermixing of structures are also supported by our data of IR reflection spectroscopy. In these investigations the most evident composition dependent behavior is observed in IR reflection spectra measured with the electric vector E parallel to the c -axis, and these changes are more apparent in the range of intrinsic vibrations of the TaO_6 octahedra, see Fig. 3. The frequencies of the transverse optical (TO) and longitudinal optical (LO) phonons for the TaO_6 vibrational modes were reported previously [13, 15, 16]. It has been found [13], that the phonon modes in the region from 590 to 870 cm^{-1} are attributed to intrinsic stretching vibrations of bonds within the TaO_6 octahedra. Thus some gradual changes of the main (i.e., common for all the LiTaO_3 crystals studied) reflectivity bands, concerning their shape and position, are observed at a variation of $[\text{Li}_2\text{O}]$ for different crystal compositions. Moreover, a Li deficiency is “marked” by a specific lattice vibration spectrum with unique characteristic reflection bands. This feature may be assigned, in our opinion, to a significant difference between the crystalline structures of the main and ilmenite-like LiTaO_3 phase, which is introduced by modified Ta–O chemical bonds with characteristic vibration frequencies. This circumstance can be used for an accurate evaluation of the Li deficiency in LiTaO_3 crystals.

A mathematical analysis of the IR reflection spectra was used to determine the TO and LO phonon frequencies. As the inflection points on the spectral dependence of the reflectivity are related to these frequencies [12, 13, 28], we calculated the spectral dependence of the first derivative $dR/d\nu$ of reflectivity R with respect to the wavenumber (frequency) ν in Fig. 4. Thus, the maxima and minima of $dR/d\nu$ correspond merely to TO and LO phonons, respectively. Note, that the minimum position is in fairly good agreement with the Raman frequency of the corresponding LO phonon, whereas the TO phonon frequency and the maximum position of $dR/d\nu$ are not well

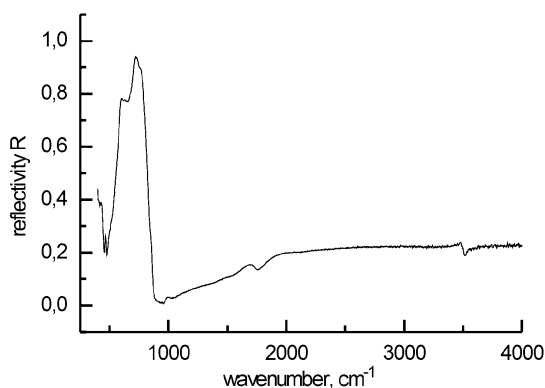


FIGURE 3 IR reflection spectra of the nearly stoichiometric sample SLT

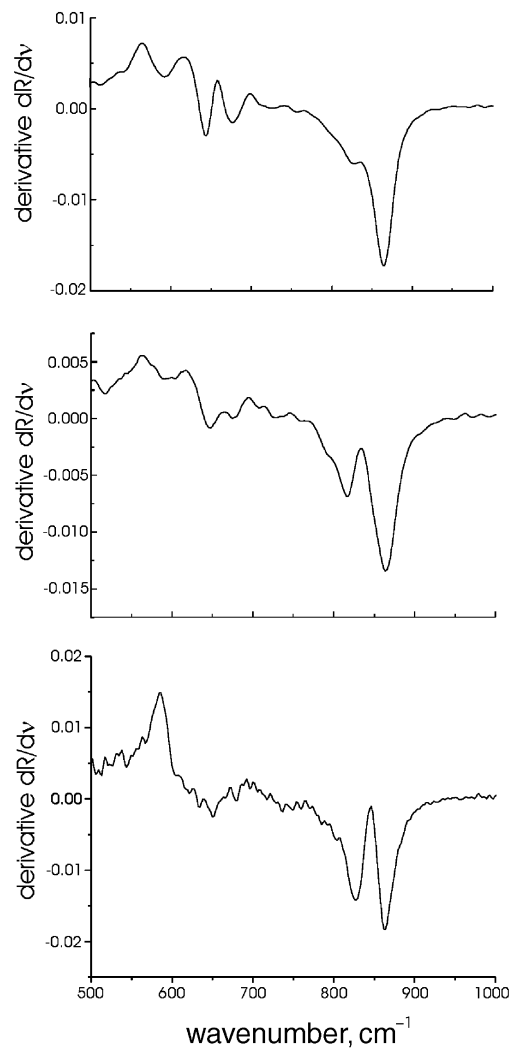


FIGURE 4 Spectral dependencies of first derivative of reflectivity $\delta R/\delta \nu$ for different LiTaO_3 crystals: (a) nearly stoichiometric sample SLT, (b) congruently melting sample CLT, and (c) quasi-congruent sample QC

correlated [13, 28]. The calculation of $dR/d\nu$ as a function of frequency ν gives precise values of the wavenumber for the extra reflection bands and allows for an accurate evaluation of their relative “intensities”, demonstrating their gradual composition dependent behavior. Such a behavior is evident for the LO phonon of the extra band observed at $820\text{--}827\text{ cm}^{-1}$, see Fig. 4. The IR reflectivity analysis demonstrates (Fig. 4a) that the nearly stoichiometric crystal has a marked concentration of intrinsic defects related to residual Li deficiency even after an intensive VTE process. At the same time, Raman spectra measurements do not give evidence of such a residual Li deficiency, as the modern Raman technique cannot resolve in principle, a difference between vibrational spectra and Raman linewidths for the crystals with 49.97 and 50.00 mol % of Li_2O .

4 Relationship between electro-optic, nonlinear optical coefficients and parameters in optical phonon spectra

Equating the electro-optic polarization to the sum of lattice and electronic contributions, we obtain the mean-

ingful relationship [10, 11] between electro-optic, Raman, and infrared oscillator parameters, which have to be summed over m :

$$n_i^2 r_{ij,k} n_j^2 = \alpha_{ij,k}^m \beta_k^m + \xi_{ijk}, \quad (1)$$

where $r_{ij,k}$ is the clamped linear electro-optic coefficient, n_i and n_j are the principal refractive indices at optical frequencies, $\alpha_{ij,k}^m \beta_k^m$ is the lattice contribution, $\alpha_{ij,k}^m$ is the differential polarizability for the mode m of an optical lattice vibration, the coefficients β_k^m can be evaluated from the infrared oscillator strength of the same mode m , and ξ_{ijk} is the electronic contribution, which can be calculated from SHG measurements.

In electro-optic measurements, E_k is produced by a low-impedance voltage source connected to electrodes on the crystal. Since the depolarizing field is effectively short-circuited, the local field is that for a TO mode and the value of $\alpha_{ij,k}^m$ at the TO phonon frequency ω_{TO}^m must be employed in (1). At frequencies well below ω_{TO}^m , β_k^m is given by $(\varepsilon_0 \Delta \kappa_k^m v / K_k^m)^{1/2}$, where ε_0 is the dielectric permeability, $\Delta \kappa_k^m$ is the contribution of the mode m to the low-frequency dielectric constant, K_k^m is the spring constant for the mode m , and v is the volume of a unit cell. Thus, using the well-known relations [11–13] for $\alpha_{ij,k}^m$ and ξ_{ijk} , we get

$$r_{ij,k} = (n_i^2 n_j^2)^{-1} \left\{ \pm [\varepsilon_0 \Delta \kappa_k^m S_{ij,k}^m / \sigma^m]^{1/2} + 4d_{ijk} \right\}, \quad (2)$$

where $S_{ij,k}^m$ is the Raman scattering efficiency for a Stokes line of mode m , σ^m is a coefficient including the Bose population factor and parameters related to experimental conditions [11], and d_{ijk} is the SHG coefficient. We define the Raman scattering efficiency as the total optical power scattered with polarization i at a Stokes frequency, divided by the total incident power with polarization j .

Thus, the study of the phonon spectrum via Raman scattering and IR reflection spectroscopy allows for an accurate determination of the lattice contribution to the electro-optic effect. It should be noted, that the pure electronic contribution $4d_{ijk}$ in the electro-optic effect in (2), which was estimated from SHG experiments, is much smaller than the lattice contribution in the case of LiTaO₃ crystals [10, 11]. This means that for a rough quantitative evaluation of the electro-optic properties of any newly developed material based on LiTaO₃, a quantitative characterization of the dominating microscopic source of the electro-optic effect related to the lattice contribution may be sufficient in some special cases [10, 13].

A theoretical modeling of the electronic structure of LiTaO₃ has demonstrated [15, 16, 31–34], that the optical properties and spontaneous polarization of LiTaO₃ may be evaluated in the frame of a quasi-molecular model, considering a TaO₆ octahedron cluster as a separate structural fragment. This cluster causes the main contribution to the spontaneous polarization P_s , which is proportional to the distortion of the octahedra in the main crystal structure LiTaO₃ [15, 31, 32]. Li vacancies and Ta ions on Li lattice sites may be essentially assumed [31] to result in a relaxation of the nearest neighbor Ta ion to the center of its surrounding O₆ octahedron, i.e., in a decrease of the TaO₆ octahedron distortion and, hence, in reduction of P_s . Moreover, it has been found [13, 31, 33], that the change of P_s caused by chem-

ical composition variation is correlated to the corresponding variation of the r_{33} electro-optic coefficient.

5 Determination of electro-optic coefficients from Raman and IR spectroscopy data

We have measured the Raman spectra related to inelastic light scattering on different phonon modes of a crystal. The selection rules in Raman spectra for varying polarizations and directions of propagation of the incident and scattered beams are determined by a third-rank differential polarizability tensor. The non-vanishing components of the differential polarizability tensor α_{ij}^k are presented below for each polar phonon mode (the direction of polarization k is indicated in parentheses):

$$A_1(z) = \begin{pmatrix} a & 0 & 0 \\ 0 & a & 0 \\ 0 & 0 & b \end{pmatrix}, \quad E(x) = \begin{pmatrix} 0 & c & d \\ c & 0 & 0 \\ d & 0 & 0 \end{pmatrix}, \quad E(y) = \begin{pmatrix} c & 0 & 0 \\ 0 & -c & d \\ 0 & d & 0 \end{pmatrix}. \quad (3)$$

Therefore, for arbitrary directions of photon and phonon propagation the dependence of the scattering efficiency S for a given Raman line on the polarization is given by [17]:

$$S_{\text{R}}^k \cong A \sum_{i,j=1}^3 [e_i \alpha_{ij}^k e_j]^2, \quad \alpha_{ij}^k = \frac{\partial \alpha_{ij}}{\partial Q_k},$$

$$S = A [e_i^x e_s^x (c \xi^y + a \xi^z) + e_i^y e_s^y (-c \xi^y + a \xi^z) + e_i^z e_s^z b \xi^z + (e_i^y e_s^z + e_i^z e_s^y) d \xi^y + (e_i^z e_s^x + e_i^x e_s^z) d \xi^x + (e_i^x e_s^y + e_i^y e_s^x) c \xi^y]^2. \quad (4)$$

In this expression e_i and e_s are the polarization vectors of the incident and scattered light, ξ is the phonon polarization, a , b , c , and d are the corresponding components of the total derivative α_{ij}^k of the macroscopic optical polarizability α_{ij} with respect to the normal mode coordinate Q_k that is specific of any Raman line, and A is a constant. The Cartesian axis Z is parallel to the c -axis, X is perpendicular to one of the three glide planes, and Y is perpendicular to X and Z .

According to (3) and (4), each optical mode polarized along the z axis (i.e. A_1 symmetry mode) contributes separately to the electro-optic coefficient r_{33} by an amount that is proportional to the product of Raman scattering efficiency and infrared oscillator strength, see the data in Table 2. Since

$\omega_j/2\pi c$, cm ⁻¹	Absolute $S_j(\text{QC})$ values	$S'(\text{UC1})$	$S'(\text{UC2})$	$S'(\text{QC})$	$S'(\text{CLT})$	$S'(\text{SLT})$
201	10.4	0.883	0.961	1	1.051	1.253
253	0.64	0.061	0.061	0.062	0.062	0.063
355	0.18	0.017	0.017	0.017	0.017	0.018
600	3.2	0.291	0.298	0.308	0.313	0.325

TABLE 2 Relative normalized values S'_j of Raman scattering efficiencies S_j of the $A_1(\text{TO})_j$ phonons measured in scattering geometry $X(\text{ZZ})X'$ for crystals with different compositions. All these values are normalized to the scattering efficiency of $A_1(\text{TO})$ phonon at 201 cm⁻¹ in a $X(\text{ZZ})\bar{X}$ spectrum of quasi-congruent crystals, i.e. $S'_j(x\text{LT}) = S_j(x\text{LT})/S_1(\text{QC})$. The data from [10] on the absolute values of $S_j(\text{QC})$ (given in 10⁻⁶ cm⁻¹sr⁻¹) were used for calibration

the contributions of the Ta–O bonds to the linear and nonlinear susceptibility are substantially larger than the corresponding contribution of Li–O bonds [31, 33, 34], we may use the following approach, taking into account the fundamental A modes of intrinsic vibrations of the TaO₆ octahedra. However, there is a principal contradiction in the data reported previously on the phonon spectrum assignment and point group symmetry of LiTaO₃. Thus, the four IR- and Raman-active z -polarized A_1 modes, corresponding to the point group symmetry C_{3v} , were observed in [10, 11, 15, 32]. In contrast, the nine IR- and Raman-active z -polarized A modes, corresponding to the point group symmetry C_3 , were observed in [16], where it has been recognized that an inherently small distortion of the unit cell induces a lowering of the crystal symmetry of LiTaO₃ from C_{3v} to C_3 . Our data on Raman (see Figs. 1 and 2) and IR reflection spectra (see Figs. 3 and 4) of congruent LiTaO₃ confirm the latter assignment, as we have observed all three A modes reported [16] for the range of 590–870 cm⁻¹, which were related to intrinsic vibrations of the TaO₆ octahedra. Besides, an extra z -polarized band at 844 cm⁻¹ is observed in IR reflection and Raman spectra of LiTaO₃. This band was reported [16] to be specific for Raman spectra of LiTaO₃, but its assignment was not clear yet. However, the analysis of our IR reflection spectra shows clearly, that this mode may be assigned to a TO phonon of some new z -polarized mode, and the corresponding LO phonon has a smaller frequency of 827 cm⁻¹, coinciding almost with the position of the inflection point on the reflectivity curve (see Fig. 4). It means, that the new mode has an inverted LO-TO splitting because of an overlapping with a mode having a larger LO-TO splitting, i.e., the main A_1 mode with a TO phonon at 596 cm⁻¹ and a LO phonon at 864 cm⁻¹. It was established by analysis of IR reflection spectra, that the LO-TO splitting of the fundamental polar A_1 mode associated with TaO₆ octahedra vibrations, which is proportional roughly to the width of the main band ranging from 596 to 864 cm⁻¹, appears to depend on the chemical composition, and it has quite different specific values for different crystals studied here, see Fig. 4. Our data show that a decrease of the LO-TO splitting for this polar mode occurs in the under-congruent LiTaO₃ crystals with high Li deficiency.

By using the data of the phonon frequencies and the Raman scattering efficiencies, the electro-optical coefficient r_{33} were estimated for all the crystals studied as presented in Table 3. The correspondence between the observed electro-optic and Raman effects can be understood as follows. We take Q_k^m as the instantaneous amplitude of a polar mode with angular frequency ω^m and lattice displacements along k , where displacements along z and normal to z correspond to A_1 and E modes, respectively. Then we define the Raman scattering efficiency S_{ijk}^m as the total optical power scattered with polarization I into a fixed angle $d\Omega$ from a length L of the crystal, divided by the total incident power with polarization j . The only non-vanishing elements in a third-rank tensor with symmetry C_{3v} are $S_{xx,z}^m = S_{yy,z}^m = S_{13}^m$, $S_{zz,z}^m = S_{33}^m$ for A modes, and $S_{xx,y}^m = S_{yy,y}^m = S_{xy,x}^m = S_{22}^m$, $S_{yz,y}^m = S_{xz,x}^m = S_{42}^m$ for E modes, where we have introduced a reduced notation for the interchangeable indices (ij).

In the Raman spectra of all three LiTaO₃ samples with different chemical compositions we found all the allowed fre-

crystal	$r_{33}^T(\text{exp})$, pm/V	r_{33}^S , pm/V	r_{33}^T , pm/V	$d_{33}(\text{exp})$, pm/V	d_{33} , pm/V
UC 1	No data	29.6	26.3	No data	22.3
UC 2	No data	~ 32.1*	~ 28.8*	No data	**
QC	30.0	33.3	30.0	26.2	26.2
CLT	32.2	~ 35.0*	~ 31.7*	26.2	**
SLT	35.5	42.3	39.0	30.4	30.7

* in these cases, accuracy of evaluation is limited by experimental conditions

** evaluation was not possible due to specific geometry of samples

TABLE 3 Values of electro-optic coefficient r_{33} (clamped r_{33}^S and unclamped r_{33}^T) and nonlinear-optical coefficient d_{33} evaluated from Raman and IR spectroscopy data. The data of direct measurements [5, 11, 17, 20] are given for comparison and denoted by “(exp)”. All the data on r_{33} are given for $\lambda = 633$ nm, and d_{33} are given for $\lambda = 1064$ nm. The direct measurement data on $r_{33}(\text{exp})$ and $d_{33}(\text{exp})$ values in quasi-congruent crystals [11, 17] have been used as calibration standards for calculation of the absolute values for electro-optic and nonlinear optical coefficients from our data. According to the known approach [11], the evaluation accuracy is estimated to be around 5% for r_{33} and 4% for d_{33}

quencies for both TO and LO modes, and most of the corresponding scattering efficiencies. The large number of intensive E mode lines present make it difficult to determine some of their Raman scattering efficiencies. Besides, according to the general law, the more lattice modes contribute, the more accurately the Raman data must be known. Therefore, the relative changes of the electro-optic coefficients r_{22} and r_{42} were not evaluated by us from Raman data, because of a low accuracy expected for such an evaluation.

It is important to note, that our Raman spectroscopy data are in good agreement with previously reported data [10, 11] on Raman scattering efficiencies for phonon modes in quasi-congruent LiTaO₃ crystals. Therefore, to estimate relative changes of the electro-optic coefficient r_{33} in any off-congruent crystals, it is sufficient to determine the relative change of the Raman scattering efficiencies and the LO-TO splittings of the A symmetry modes with respect to a congruent crystal. The two A modes, having frequencies of the TO phonons of 661 and 751 cm⁻¹, demonstrate a very small LO-TO splitting in any sample independently of its chemical composition. It means, according to (3) and (4), that the contribution of these modes to the electro-optic effect is not significant. Such contribution, therefore, has been neglected in our calculations. Thus, we take into account the four fundamental A modes assigned [10–13] to A_1 symmetry in pure LiTaO₃ and the extra A mode with the TO phonon frequency at 844 cm⁻¹. The obtained results point to a degradation of the electro-optic properties in the under-congruent crystals, which will limit their use for electro-optic devices.

Note, that the electro-optical coefficient r_{33} obtained here for the nearly stoichiometric crystals is larger than those estimated from direct measurements [20], see Table 3. This may be attributed to the effect of an internal field, averaging over a non-uniform ferroelectric material and decreasing the “effective” value of $r_{ij,k}$ when using direct methods based on an electro-optical modulator arrangement. However, the Raman scattering method provides information about local changes of dipoles, which are responsible for the electro-optical effect, and thus this method is insensitive to averaging effects.

At the same time, the Raman spectroscopy allows only for the evaluation of high-frequency values of $r_{ij,k}$, i.e. the so-

called clamped electro-optic coefficient r^S , but does not give any information about the piezo-optic contribution caused by acoustic resonances in the low-frequency range. Nevertheless, it contributes to the effective value of r_{ijk}^T measured under unclamped experimental conditions, i.e. with applied electric fields ranging from dc to acoustic resonances frequencies [35]. Hence, the acoustic contribution r^a may be evaluated from the difference between unclamped and clamped electro-optic coefficients $r^a = r^T - r^S$. Comparison of our results with the data of a direct measurement of r_{33}^S and r_{33}^T in quasi-congruent and nearly stoichiometric crystals has shown, according to the data [35] on dispersion of r_{33} in quasi-congruent LiTaO₃, that the growth of the effective electro-optic coefficients for a change of chemical composition from quasi-congruent to nearly stoichiometric is caused mainly by alteration of ionic contributions related to optical phonons. This finding is valid even within the low-frequency range, demonstrating a small change of the acoustic contribution at such a composition variation. It allows us to assume the same behavior at the transition from quasi-congruent to under-congruent composition. Thus, we conclude that the effective unclamped electro-optic coefficients r_{33}^T and r_c^T ($r_c = r_{33} - [n_o/n_e]^3 r_{13}$) should have rather smaller values in under-congruent crystals compared to the congruent and nearly stoichiometric crystals. Note, that no data has been published yet for a direct electro-optic measurement in under-congruent crystals, i.e. our results present a first evaluation of electro-optic properties of this material.

6 Composition dependence of nonlinear-optic coefficients

To determine the pure electronic contribution $\xi_{ijk} = 4d_{ijk}$ in the electro-optic effect in (1) and (2) and, hence, to evaluate the value of the nonlinear optical coefficients d_{ijk} , we have measured the difference between Raman scattering efficiencies of LO and TO phonons for each mode, as the following expression is valid for LiTaO₃ crystals [10, 11]:

$$\Sigma(S_{ij,m}^L - S_{ij,m}^T) = -32\pi \Sigma(\epsilon_\infty^{-1})^{\gamma\beta} Z_m^\beta d_{ij,\gamma} \alpha_{ijm} + 256\pi^2 \Sigma \left[(\epsilon_\infty^{-1})^{\gamma\beta} Z_m^\beta d_{ij,\gamma} \right]^2, \quad (5)$$

where Z_m^β is an element of the effective transverse charge-parameter matrix for a mode with index m and polarization direction β , and Z_m^β is related to the dielectric response function by equation [11]:

$$\epsilon^{\gamma\beta}(\omega) = \epsilon_\infty^{\gamma\beta} + \Sigma \left[(4\pi Z_m^\gamma Z_m^\beta) / (\omega_m^2 - \omega^2) \right]. \quad (6)$$

For LiTaO₃, because of its point group symmetry, the principal axes correspond to the crystallographic axes and the modes with $Z_m^\beta \neq 0$ (or $Z_m^\gamma \neq 0$) may be grouped by axis β , since only one of the three Z_m^β component is $\neq 0$ for each m , i.e., Z_m^β splits from a $3N \times 3$ to three $N \times 1$ matrices. Thus, $\beta, \gamma = 1, 2, 3$, where the index 3 corresponds to the optical axis and, hence, in (5) and (6) denotes the parameters for A symmetry modes.

From our experimental measurements, we observe that Raman scattering efficiencies are generally weaker for LO

than for TO modes, and the difference between these efficiencies depends on the chemical composition: the difference becomes larger when [Li₂O] increases. Because we have studied quantitatively such a difference for only three different compositions, our data is not sufficient to establish an exact law for the composition dependence of Raman efficiencies. It is worth to notice that our Raman data, and by use of (5), allows for an evaluation of the nonlinear optical coefficient d_{33} values in all three crystals. The obtained data is given in Table 3. The relative values are 0.85, 1, and 1.17 in under congruent, quasi-congruent (used as reference value), and nearly stoichiometric crystals, respectively [14, 15]. Using the data of the absolute value of $d_{33} = 26.2$ pm/V reported for standard nominally pure quasi-congruent LiTaO₃ [17, 23], we find d_{33} to be 22.3 and 30.7 pm/V in under congruent and nearly stoichiometric crystals, respectively. This estimation is in good agreement with data on direct measurements [20]. Therefore, we assume, that our present approach may be extended for LiTaO₃ crystals with any compositions within the entire composition range of the lithium tantalate phase. Finally, we conclude that the determination of nonlinear optical coefficients of unknown LiTaO₃ samples from Raman and IR reflection data can indeed be practical, particularly as an alternative when a direct measurement is impossible or inconvenient.

7 Summary and conclusions

The data presented shows that both the Raman scattering method and IR reflection spectroscopy are well suitable techniques for a simple, nondestructive and fast determination of chemical composition, electro-optic coefficients, and nonlinear optical coefficients of LiTaO₃ crystals. These methods exhibit rather good accuracy, both relative and absolute. No restrictions have been found for the composition range of LiTaO₃ in which the techniques are applicable. The obtained electro-optic and nonlinear optical coefficients have been compared with values obtained by direct measurements in quasi-congruent and nearly stoichiometric crystals. The good agreement of our data with these measurements opens up a new possibility for fast and easy estimation of the nonlinear performance of any newly developed LiTaO₃-based material, allowing also for the investigation of small and non-perfect samples. Furthermore, structure intermixing has been recognized to be a specific feature of any nonstoichiometric crystals, even for nearly stoichiometric ones. Here the Raman and IR reflection data allow assumption of the existence of ilmenite-like structures in Li deficient LiTaO₃ crystals.

REFERENCES

- 1 A.M. Glass, G.E. Peterson, T.J. Negran, In: *Laser Induced Damage in Optical Materials*, ed. by A.M. Glass, A.H. Guenter (Nat. Bur. Stand., Spec. Publ. Vol. 372, Washington, DC 1972) pp. 15–26
- 2 W.B. Spillman, N.A. Sanford, R.A. Soref, *Opt. Lett.* **8**, 497 (1983)
- 3 T. Findakly, P. Suchoski, F. Leonberger, *Opt. Lett.* **13**, 797 (1988)
- 4 D.B. Maring, S.M. Kostritskii, R.F. Tavlykaev, R.V. Ramaswamy, *Proc. IPR (OSA)*, 281 (1999)
- 5 Y.S. Kuz'minov, *Lithium Niobate and Lithium Tantalate Crystals* (Nauka, Moscow 1975) p. 224
- 6 P.F. Bordui, R.G. Norwood, C.D. Bird, J.T. Carella, *J. Appl. Phys.* **78**, 4647–4650 (1995)

- 7 V. Gopalan, N. Sanford, J.A. Aust, K. Kitamura, Y. Furukawa, *Recent Advances in the Crystal Growth Characterization and Domain Studies in Lithium Niobate and Lithium Tantalate Ferroelectrics*, In: Handbook of advanced electronic and photonic materials, H. Singh Nalwa (ed.) (Acad. Press 2000) p. 57
- 8 C. Bäumer, C. David, A. Tunyagi, K. Betzler, H. Hesse, E. Krätzig, M. Wöhlecke, *J. Appl. Phys.* **93**, 3102 (2003)
- 9 C. Bäumer, C. David, K. Betzler, H. Hesse, K. Lengyel, L. Kovács, M. Wöhlecke, *Phys. Stat. Solidi A* **201**, R13 (2004)
- 10 I.P. Kaminow, W.D. Johnston, *Phys. Rev.* **160**, 519 (1967)
- 11 W.D. Johnston, *Phys. Rev. B* **1**, 3494 (1970)
- 12 A.S. Barker R. Loudon, *Phys. Rev.* **158**, 433 (1968)
- 13 S.M. Kostritskii, D.B. Maring, R.F. Tavlykaev, R.V. Ramaswamy, Y.N. Korkishko, V.A. Fedorov, *J. Appl. Phys.* **91**, 930 (2002)
- 14 B.A. Scott, G. Burns, *J. Am. Ceram. Soc.* **55**, 225 (1972)
- 15 C. Rocchiccioli-Deltcheff, R. Franck, *Seminaires Chim. Etat. Sol.*, 7, J.P. Suchet (ed.) (Masson et Cie S.A., Paris 1974) pp. 43–65
- 16 A.F. Penna, A. Chaves, P.R. Andrade, S.P.S. Porto, *Phys. Rev. B* **13**, 4907 (1976)
- 17 Lithium Tantalate, Select technical data. Deltronic Crystal Industries, Inc. (1999)
- 18 J. Imbrock, C. Bäumer, F. Holtmann, H. Hesse, E. Krätzig, D. Kip, TOPS, Vol. 87, Nice, France, 14–18 July (2003) p. 15
- 19 A. Wirp, C. Bäumer, H. Hesse, D. Kip, E. Krätzig, *Phys. Stat. Solidi A* **202**, 1120 (2005)
- 20 Opto-single crystal research group, www.nims.go.jp/osc/
- 21 YCC Specifications, Vides Roditi Int. (2004)
- 22 U. Schlarb, S. Klauer, M. Wesselmann, K. Betzler, M. Wöhlecke, *Appl. Phys. A* **56**, 311 (1993)
- 23 D.H. Jundt, M.M. Fejer, R.L. Bayer, *IEEE J. Quantum Electron.* **26**, 135 (1990)
- 24 A. Bruner, D. Eger, S. Ruschin, *J. Appl. Phys.* **96**, 7445 (2004)
- 25 O.F. Schirmer, O. Thiemann, M. Wöhlecke, *J. Phys. Chem. Solids* **52**, 185 (1991)
- 26 H. Donnerberg, S.M. Tomlinson, C.R.A. Catlow, O.F. Schirmer, *Phys. Rev. B* **40**, 11909 (1989)
- 27 S.M. Kostritskii, O.G. Sevostyanov, *Appl. Phys. B* **65**, 527 (1997)
- 28 H. Poulet, J.P. Mathieu, *Spectres de Vibration et Symetrie des Cristaux* (Gordon and Breach, Paris, NY 1970)
- 29 S.M. Kostritskii, P. Moretti, *Radiat. Eff. Defect. S* **150**, 151 (1999)
- 30 M.A. McCoy, S.A. Dregia, W.E. Lee, *J. Mater. Res.* **9**, 2029 (1994)
- 31 H. Ahlfeldt, J. Webjorn, P.A. Thomas, S.J. Teat, *J. Appl. Phys.* **77**, 4467 (1995)
- 32 K.A. Muller, Y. Luspain, J.L. Servoin, F. Gervais, *J. Phys. Lett.-Paris* **43**, L537 (1982)
- 33 S.H. Wemple, M. Di Domenico, *J. Appl. Phys.* **40**, 720 (1969)
- 34 S.H. Wemple, M. Di Domenico, I. Camlibel, *Appl. Phys. Lett.* **12**, 209 (1968)
- 35 M. Abarkan, J.P. Salvestrini, M.D. Fontana, M. Aillerie, *Appl. Phys. B* **76**, 765 (2003)
- 36 K. Kitamura, Y. Furukawa, K. Niwa, V. Gopalan, T.E. Mitchell, *Appl. Phys. Lett.* **73**, 3073 (1998)